Stub model for charge transport through a quantum dot connected to noncollinear ferromagnets

S. Rodríguez-Pérez, A. L. R. Barbosa, and A. M. S. Macêdo
Departamento de Física, Laboratório de Física Teórica e Computacional, Universidade Federal de Pernambuco, 50670-901 Recife, Pernambuco, PE, Brazil

(Received 30 October 2009; revised manuscript received 25 January 2010; published 19 February 2010)

A stub model is introduced to describe the charge transport properties of a system consisting of an arbitrary number of noncollinear ferromagnetic or normal reservoirs coupled nonideally to a normal metal chaotic cavity. We characterize the contacts by a reduced set of parameters which can be used to express the average value of any charge-transfer cumulant. Explicit expressions of this set of parameters are given for the cases of ideal ballistic contacts and tunnel junctions. The average conductance and shot-noise power of a two terminal FNF device with noncollinear ferromagnetic reservoirs are calculated analytically via an extended diagrammatic method which allows for the importation of all diagrams of the corresponding NNN system. We observe that the Fano factor exhibits a transition between monotonic and nonmonotonic behaviors as a function of the reservoir's relative magnetization angle. A diagram of this transition in the plane of the polarization parameters is shown. With straightforward modifications, our scheme paves the way for efficient calculations of the average value of an arbitrary cumulant of the charge-transfer statistics in hybrid devices along with its quantum corrections.

DOI: 10.1103/PhysRevB.81.085326 PACS number(s): 73.23.−b, 73.21.La, 72.25.−b

I. INTRODUCTION

The great technological potential of magnetoelectronic systems[1] have attracted the interest of many condensed matter physicists in the last two decades. Particularly, noncollinear magnetoelectronics has been an active subarea in recent years.[2] Phenomena such as angular magnetoresistance and spin-transfer torque[3] have stimulated the proposal of novel devices such as spin-flip and spin-torque transistors.[2,4]

Building on the finite element approach to superconductor—normal metal hybrid systems,[5] Brataas *et al.* proposed a circuit theory (CT) for noncollinear magnetotransport,[6] in which the system is represented as a network containing three kinds of elements: nodes, reservoirs, and connectors. The nodes and the reservoirs are described by local distribution functions, while the connectors are characterized by a set of experimentally controllable parameters. Because of the great quantity of microscopic information, irrelevant as far as some transport properties are concerned, which are cutoff by construction, the formal manipulation in this formalism is relatively simple even for complex systems. Using this approach, the average spin and charge currents have been calculated under various experimentally relevant conditions.[2] An extension of circuit theory that accounts for shot noise was put forward in Ref. 7. More recently, a semiclassical Boltzmann-Langevin theory was presented to describe a normal diffusive metal connected to ferromagnetic reservoirs via tunnel contacts[8] and the shot-noise power was calculated taking into account spin-flip scattering in the normal metal.

A common feature of these approaches is that they are based on semiclassical schemes, which although quite suitable for the description of conventional spintronic devices may become inadequate for modern devices, such as those based on semiconductors,[9] where quantum interference effects have been observed.[10,11] A fully quantum-mechanical approach was presented by Waintal *et al.* in a scattering matrix framework.[12] They used random matrix theory (RMT) to calculate the current-induced torque in an FNF system. While this theory has as starting point the complete scattering matrices of the FN interfaces, the final results can be expressed as a function of only a few number of parameters, thus showing that it contains a great amount of redundant information. Building on some results of this approach, a theoretical scheme, denoted continuous random matrix theory, has recently been proposed.[13] It carefully removes the irrelevant microscopic information for the calculation of the average spin and charge currents through the introduction of some effective parameters and provides a conceptual connection between quantum and classical approaches such as circuit theory.

For normal systems with two terminals the circuit theory equations for the generating function of charge-transfer cumulants were derived from the semiclassical limit of the scattering approach, both from a diagrammatic perturbative expansion based on RMT (Ref. 14) and from the saddle-point equation of the corresponding supersymmetric nonlinear sigma model.[15] This connection can be used as a systematic tool to remove the redundancy of the random matrix description via an exact map onto the appropriate nonlinear sigma model, which contains only the relevant large scale degrees of freedom.

Motivated by the observation of interference effects in semiconductor-based spintronic devices and by the above described redundancy removal scheme, we propose in this work a stub model that combines the simplicity of circuit theory with the generality of the RMT-based scattering approach. We demonstrate these features by explicitly calculating the average conductance and the average shot-noise power of an FNF system in the regime of phase coherent transport. We observe that the Fano factor exhibits a transition between monotonic and nonmonotonic behaviors as a function of the reservoir's relative magnetization angle. A diagram of this transition in the plane of the polarization parameters is shown. Our formalism also provides a proce-

dure to select a reduced set of parameters for each type of contact which can be used to characterize the average value of any observable that can be expressed as a linear statistics on the transmission eigenvalues such as the cumulants of charge-transfer statistics. Explicit expressions for the set of relevant parameters in the case of ideal ballistic contacts and tunnel junctions are presented. Finally, our approach can be easily extended to yield a systematic algorithm for the calculation of the average value of higher-order charge-transfer cumulants along with quantum interference effects such as the weak localization correction.

The article is organized as follows. In Sec. II we describe the physical system and introduce the stub model. In Sec. III we define the reduced set of parameters that are needed to express any planar diagram of the perturbative semiclassical expansion. Explicit expressions are given for ideal ballistic contacts and tunnel junctions. Section IV is devoted to explain the introduction of the spin degrees of freedom in the diagrams. The average conductance and the average shot-noise power are calculated for an FNF system. We show that the Fano factor exhibits a transition between monotonic and nonmonotonic behavior as a function of the reservoir's relative magnetization angle. A diagram of this transition in the plane of the polarization parameters is shown. A summary and conclusions are presented in Sec. V.

II. STUB MODEL

Our model system consists of a normal metal chaotic cavity connected nonideally to an arbitrary number of ferromagnetic or normal reservoirs. For the sake of generality, we shall consider the ith reservoir to be characterized by a magnetization $\vec{m}_i$ and connected to a single node through an arbitrary type of contact. The system is assumed to be removed from equilibrium by the application of a bias voltage and charge transport takes place in the linear regime. The terminals are supposed to be kept in local equilibrium thus giving rise to a stationary process. We will neglect any spin-flip process in both the cavity and the contacts and thus the dwell time of electrons in the cavity is assumed to be much smaller than the spin-flip time, $\tau_{dwell} \ll \tau_{sf}$. We also assume that the dwell time is much bigger than the ergodic time, $\tau_{dwell} \gg \tau_{ergodic}$, so that the quantum dynamics inside the cavity is in the universal chaotic regime. Finally, we ignore any inelastic process during the observation time, and therefore the charge transport is fully phase coherent.

Since we are concerned with a hybrid metallic system, we assume the number of open scattering channels to be large so that a semiclassical description is justifiable and quantum interference corrections can be safely neglected. In the language of the diagrammatic technique, this means that we are interested in a selected class of planar diagrams associated with the dominant semiclassical contribution of the average charge transfer cumulants in a perturbative expansion. This particular class is indifferent to the presence or the absence of time reversal symmetry (TRS) in the system.

The central idea of our formalism is to represent the chaotic cavity as a noise generating stub, which is described by a random unitary matrix from the appropriate circular ensemble. Stub models have had great success in the random matrix description of quantum transport, allowing for the inclusion of a variety of effects such as the presence barriers,[16] crossovers between universality classes,[17] and time dependence.[18] It can be shown[16] that the total scattering matrix S and the scattering matrix of the cavity S_0 are related via the following matrix stochastic equation

$$S = \bar{S} + T'(1 - S_0 R)^{-1} S_0 T, \tag{1}$$

where

$$\begin{Bmatrix} \bar{S}_{ij} \\ R_{ij} \\ T_{ij} \\ T'_{ij} \end{Bmatrix} = \delta_{ij} \times \begin{Bmatrix} \hat{r}_i \\ \hat{r}'_i \\ \hat{t}_i \\ \hat{t}'_i \end{Bmatrix}. \tag{2}$$

Here $\bar{S}$ denotes the ensemble average of S, $\hat{r}_i$, $\hat{r}'_i$, $\hat{t}_i$, and $\hat{t}'_i$ are $2N_i \times 2N_i$ reflection and transmission matrices of the ith contact with N_i open channels and the hat indicates the presence of the spin structure. The basic constraint of the stub formalism is that the matrix

$$\Sigma = \begin{pmatrix} \bar{S} & T' \\ T & R \end{pmatrix}, \tag{3}$$

must be unitary. All matrices in Eq. (1) are $2N_T \times 2N_T$, where N_T is the total number of open channels and the factor 2 accounts for spin.

If the angle between the quantization axis (which will be chosen as the z axis) and the direction of the magnetization $\vec{m}_i$ is θ_i, the elements of the scattering matrix of the ith contact have to be rotated about the direction defined by $\hat{n}_i = \hat{k} \times \vec{m}_i / \sin\theta_i$ by using a U(2) operation.[12] The reflection matrix, for example, is rotated as

$$\hat{r}_i(\hat{n}_i, \theta_i) = \hat{R}_i(\hat{n}_i, \theta_i) \hat{r}_i(0) [\hat{R}_i(\hat{n}_i, \theta_i)]^\dagger, \tag{4}$$

where

$$\hat{R}_i(\hat{n}_i, \theta_i) = \mathrm{I}_{N_i} \otimes \left[\mathrm{I}_2 \cos\left(\frac{\theta_i}{2}\right) - i\vec{\sigma} \cdot \hat{n}_i \sin\left(\frac{\theta_i}{2}\right) \right], \tag{5}$$

$$\hat{r}_i(0) = \begin{pmatrix} r_i^{\uparrow} & 0 \\ 0 & r_i^{\downarrow} \end{pmatrix}, \tag{6}$$

and $\vec{\sigma}$ is a vector whose components are the Pauli matrices. The identity matrix I_{N_i}, $r_i^{\uparrow}$, and $r_i^{\downarrow}$ are $N_i \times N_i$ matrices. The off diagonal elements of $\hat{r}_i(0)$ are null because we neglect spin-flip processes.

We have assumed the cavity to be a normal metal and its internal dynamics to be in the universal chaotic regime, therefore we can model our noise source, the scattering matrix S_0, as follows

$$S_0 = U \otimes \mathrm{I}_2. \tag{7}$$

Here I_2 is the identity matrix in spin space and U is a $N_T \times N_T$ random matrix from the circular unitary ensemble (CUE).[19] Therefore S_0 belongs to a subgroup of $\mathbf{U}(2N_T)$ with uniform probability distribution

$$P(S_0) = P(U) = \text{const.} \tag{8}$$

It follows from Eqs. (1) and (8) that S is distributed according to the Poisson kernel,[20] which in turn implies that any statistical property of a transport observable can be written as a function of $\bar{S}$ only.

By selecting a representation in which S_0 is block diagonal, as in Eq. (7), we maximize the efficiency of the diagrammatic rules for averaging over the unitary group. The price to pay is that the other matrices in Eq. (1) have to be transformed to this representation as well, and in this way they become nondiagonal in spin space, since by assumption at least one of the angles θ_i is nonvanishing. This is a feature of noncollinear transport. When the device has just two terminals, the change in representation can be performed by means of the following unitary matrix

$$\mathcal{U} = \begin{pmatrix} \mathrm{I}_{N_a} & 0 & 0 & 0 \\ 0 & 0 & \mathrm{I}_{N_b} & 0 \\ 0 & \mathrm{I}_{N_a} & 0 & 0 \\ 0 & 0 & 0 & \mathrm{I}_{N_b} \end{pmatrix}. \tag{9}$$

The extension of $\mathcal{U}$ to the case of a multiterminal device is straightforward. The nondiagonality in spin space of the matrices mentioned above will bring about some important implications in applying the diagrammatic method, as we shall describe shortly.

III. RELEVANT PARAMETERS

From all the information contained in the scattering matrices of the contacts, just a set of experimentally controllable parameters are needed to characterize the quantum transport properties of the device. Frequently this set contains only the transmission eigenvalues, i.e., the eigenvalues of $\hat{t}\hat{t}^\dagger$, where $\hat{t}$ is the transmission matrix.[21] The situation is more complex in noncollinear magnetoelectronics because of the loss of commutativity of certain matrices in the extended spin-channel space. In circuit theory this leads to the introduction of a 2×2 conductance matrix and a 4×4 noise matrix for the characterization of the ith connector as follows:

$$G_i^{s_1 s_1'} = \mathrm{Tr}[\mathrm{I}_{N_i} - r_i^{s_1}(r_i^{s_1'})^\dagger],$$

$$s_i^{s_1 s_1' s_2 s_2'} = \mathrm{Tr}[\mathrm{I}_{N_i} - r_i^{s_1}(r_i^{s_1'})^\dagger r_i^{s_2}(r_i^{s_2'})^\dagger]. \tag{10}$$

These parameters are essential ingredients to the calculation of the conductance[6] and shot-noise power[7] using CT.

It can be shown that only some invariants under U(2) transformations are necessary to express the information content of a planar diagram. This is a consequence of the noncrossed topology of this type of diagram. The symmetry operations can be represented as

$$\mathcal{R}_{i,j} = \delta_{i,j}\hat{R}_i(\hat{n}_i, \theta_i). \tag{11}$$

These invariants are general quantities of the form (denoted γ parameters for brevity)

$$\gamma_i^{s_1 s_1' s_2 s_2' \ldots s_n s_n'} = \mathrm{Tr}[r_i^{s_1}(r_i^{s_1'})^\dagger r_i^{s_2}(r_i^{s_2'})^\dagger \ldots r_i^{s_n}(r_i^{s_n'})^\dagger]. \tag{12}$$

It is a known theorem[22] that the invariants under similarity transformations of a $k\times k$ matrix are determined by the trace of the first k powers of the matrix. Therefore, only the parameters $\gamma_i^{s_1 s_1' s_2 s_2' \ldots s_n s_n'}$ with $n \leq 2N_i$ are independent.

There is a simple relation between the tensors $\gamma_i^{s_1 s_1'}$ and $\gamma_i^{s_1 s_1' s_2 s_2'}$ on one hand and the conductance matrix $G_i^{s_1 s_1'}$ and the noise matrix $s_i^{s_1 s_1' s_2 s_2'}$ on the other. We find

$$\gamma_i^{s_1 s_1'} = N_i - G_i^{s_1 s_1'},$$

$$\gamma_i^{s_1 s_1' s_2 s_2'} = N_i - s_i^{s_1 s_1' s_2 s_2'}, \tag{13}$$

where N_i is the number of open channels in the ith lead.

Following the conventions of Refs. 7 and 23 let us now show explicit expressions for the γ parameters in the particular cases of ideal ballistic contacts and tunnel junctions. In the first case we have

$$\gamma_i^{\downarrow\downarrow\ldots\downarrow} = \gamma_i^{\downarrow\downarrow} = \frac{g_i}{2}(1 + p_i), \tag{14}$$

while for any other combination of the indices s_k, s_k' we have

$$\gamma_i^{s_1 s_1' s_2 s_2' \ldots s_n s_n'} = \gamma_i^{\uparrow\uparrow} = \frac{g_i}{2}(1 - p_i), \tag{15}$$

where $g_i = N_i^\uparrow + N_i^\downarrow$ and $p_i = (N_i^\uparrow - N_i^\downarrow)/g_i$. $N_i^\uparrow$ and $N_i^\downarrow$ are the number of open channels for spin up and down, respectively. We have considered without loss of generality that $N_i^\uparrow > N_i^\downarrow$.

In the case of a tunnel junction, we obtain

$$\gamma_i^{s_1 s_1' s_2 s_2' \ldots s_n s_n'} = \sum_{k=1}^{n} \gamma_i^{s_k s_k'} - (n-1)N_i, \tag{16}$$

where $\gamma_i^{s_k s_k'}$ are the elements of the matrix

$$\hat{\gamma}_i = \begin{pmatrix} N_i - \frac{g_i}{2}(1 + p_i) & N_i - \frac{g_i}{2} \\ N_i - \frac{g_i}{2} & N_i - \frac{g_i}{2}(1 - p_i) \end{pmatrix},$$

where $g_i = G_i^\uparrow + G_i^\downarrow$, $p_i = (G_i^\uparrow - G_i^\downarrow)/g_i$, and $G_i^\uparrow (G_i^\downarrow)$ are the conductance of the up (down) channel and is denoted by G_i^{ss} in Eq. (10). Note that there are just two free γ parameters for a ballistic contact, while tunnel junctions are characterized by three independent γ parameters.

IV. AVERAGING OVER THE UNITARY GROUP

In order to calculate physical observables from the theory, we need to average functions that are traces in both channel and spin spaces, involving random S_0 matrices. There is a diagrammatic method for averaging over the unitary group, which was thoroughly presented and extensively applied in Ref. 16. Here, we adapt it to our problem. From Eq. (7) we can write

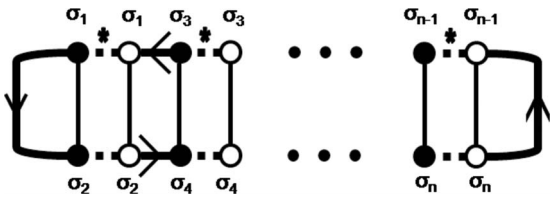

FIG. 1. Typical ladder diagram from the conductance calculation. Einstein summation convention is adopted for the spin indices.

$$(S_0)_{ij,nm,\sigma_1\sigma_2} = U_{ij,nm}\delta_{\sigma_1\sigma_2}, \tag{17}$$

where the indices i,j, n,m, and σ_1,σ_2 label direction of propagation, channel, and spin structure, respectively. The trace in the spin structure and the δ function, shown in Eq. (17), bring two additional features to the diagrammatic rules of normal systems. First, it is necessary to label the dots of a diagram, that are connected by thick dotted lines with the same spin label (see, e.g., Fig. 1). Second, a sum over all spin indices must be performed at the end of the calculation. The first feature implies, in the diagrammatic language, that all T cycles are tensors with respect to the U(2) group.

We are now in position to calculate the average conductance and shot-noise power of a two terminal FNF system. We consider the ferromagnetic reservoirs to have magnetizations whose directions are $\vec{m}_a$ and $\vec{m}_b$ and we choose $\vec{m}_a$ parallel to the z axis. The vector $\vec{m}_b$ is considered to be in the $x-z$ plane, so we have to perform the rotation of the scattering matrix of the contact b about the y axis, thus $\hat{n}=\hat{y}$.

A. Conductance

The Landauer-Buttiker formula for the zero temperature conductance reads as

$$G = G_0\,\hat{\mathrm{Tr}}(\hat{t}\hat{t}^{\dagger}), \tag{18}$$

where $G_0=e^2/h$ is the conductance quantum, $\hat{t}$ is the transmission matrix of the system, and the symbol $\hat{\mathrm{Tr}}$ stands for the trace over both channel and spin spaces. Bearing in mind the transformation shown in Eq. (9) we express the averaged conductance as

$$\langle G\rangle = G_0\langle\hat{\mathrm{Tr}}(C_a\delta S C_b\delta S^{\dagger})\rangle, \tag{19}$$

where $\delta S \equiv S-\bar{S}$ and C_a, C_b are projectors defined as

$$C_a = \begin{pmatrix} \mathrm{I}_{N_a} & 0 & 0 & 0 \\ 0 & 0 & 0 & 0 \\ 0 & 0 & \mathrm{I}_{N_a} & 0 \\ 0 & 0 & 0 & 0 \end{pmatrix}, \tag{20}$$

and

$$C_b = \begin{pmatrix} 0 & 0 & 0 & 0 \\ 0 & \mathrm{I}_{N_b} & 0 & 0 \\ 0 & 0 & 0 & 0 \\ 0 & 0 & 0 & \mathrm{I}_{N_b} \end{pmatrix}. \tag{21}$$

Inserting Eq. (1) into Eq. (19), expanding in powers of S_0 and performing the ensemble average we obtain a sum of ladder diagrams of the form shown in Fig. 1. The directed thick solid line on the left (right) extreme represents the spin-space elements of the matrix $A=(T')^{\dagger}C_aT'$ and $(B=TC_bT^{\dagger})$. The directed thick solid bottom lines in the middle (top lines in the middle) represent spin-space elements of the matrix R $(R^{\dagger})$. From now on we shall adopt Einstein's summation convention for spin indices. The information content of the diagrams can be conveniently represented in terms of vectors and matrices defined via the following prescription.

Any quantity of the form $\mathrm{Tr}(X_{\sigma_1\sigma_2})$ can be regarded as a vector $\mathcal{X}=(\mathrm{Tr}\,X_{1,1},\mathrm{Tr}\,X_{1,2},\mathrm{Tr}\,X_{2,1},\mathrm{Tr}\,X_{2,2})$. Similarly, quantities such as $\mathrm{Tr}(Y_{\sigma_1\sigma_2}Z_{\sigma_3\sigma_4})$ can be organized as 4×4 matrices $\mathcal{Y}_{s_1s_2}$ or as 1×16 vectors $\mathcal{Y}_s$. In the first case the rows s_1 are determined by the ordered pair of indices (σ_1,σ_4) and the columns s_2 by (σ_2,σ_3). In the latter case the first pair of indices run prior to the last pair. With these conventions, we define the matrix

$$\mathcal{L}_{s_1s_2} \equiv \mathrm{Tr}(R_{\sigma_1\sigma_2}R^{\dagger}_{\sigma_3\sigma_4}), \tag{22}$$

and the vectors

$$\mathcal{A}_s \equiv \mathrm{Tr}\,A_{\sigma_1\sigma_2},$$

$$\mathcal{B}_s \equiv \mathrm{Tr}\,B_{\sigma_1\sigma_2}. \tag{23}$$

Performing the summation over ladder diagrams, we obtain the following compact expression for the average conductance:

$$\frac{\langle G\rangle}{G_0} = \mathcal{A}\cdot(N_T\mathrm{I}_4-\mathcal{L})^{-1}\cdot\mathcal{B}^{\top}, \tag{24}$$

where $\mathcal{A}=(G_a^{\uparrow\uparrow},0,0,G_a^{\downarrow\downarrow})$ and $\mathcal{B}=(\mathcal{B}_1,\mathcal{B}_2,\mathcal{B}_3,\mathcal{B}_4)$ with

$$\mathcal{B}_1 = G_b^{\uparrow\uparrow}\cos^2\frac{\theta}{2} + G_b^{\downarrow\downarrow}\sin^2\frac{\theta}{2}, \tag{25}$$

$$\mathcal{B}_2 = \sin\frac{\theta}{2}\cos\frac{\theta}{2}(G_b^{\uparrow\uparrow}-G_b^{\downarrow\downarrow}), \tag{26}$$

$$\mathcal{B}_3 = \sin\frac{\theta}{2}\cos\frac{\theta}{2}(G_b^{\uparrow\uparrow}-G_b^{\downarrow\downarrow}), \tag{27}$$

$$\mathcal{B}_4 = G_b^{\uparrow\uparrow}\sin^2\frac{\theta}{2} + G_b^{\downarrow\downarrow}\cos^2\frac{\theta}{2}. \tag{28}$$

The superscript $\top$ stands for the transpose operation and the matrix $\mathcal{L}$ is shown in the Appendix. The simplicity of Eq. (24) is already a demonstration of the tractability of the stub model. By contrast, other approaches give equivalent, but much more complicated expressions. In Fig. 2 we show the

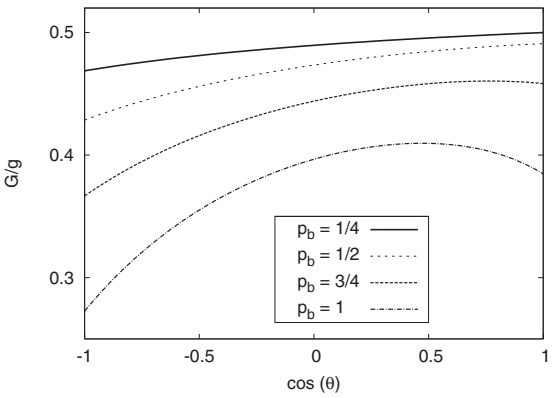

FIG. 2. Angular dependence of the average conductance in units of $g=G^{\uparrow}+G^{\downarrow}$. The value of the parameters are $g_a=g=g_b$, $G_a^{\uparrow\downarrow}=g=G_b^{\uparrow\downarrow}$, and $p_a=1/4$.

angular dependence of the conductance in units of $g=G^{\uparrow}+G^{\downarrow}$ for asymmetric contacts. The free parameters are fixed as follows $g_a=g=g_b$, $G_a^{\uparrow\downarrow}=g=G_b^{\uparrow\downarrow}$, and $p_a=1/4$. We observe a nonmonotonic behavior of the conductance as p_b grows, as reported in Ref. 24. For identical contacts, the expression for the conductance reads as

$$\langle G\rangle = \frac{g}{2}\left[1 - p^2 \frac{\tan^2\frac{\theta}{2}}{\tan^2\frac{\theta}{2} + |\eta|^2/\mathrm{Re}(\eta)}\right], \tag{29}$$

where $\eta=2G^{\uparrow\downarrow}/g$, in agreement with the result obtained in Ref. 6 using circuit theory.

B. Shot-noise power

The main technical appeal of our approach is the possibility to calculate efficiently the average of any charge-transfer cumulant within the same framework. Here, we shall demonstrate this by calculating the average second cumulant, which is the shot-noise power. In the scattering formalism the zero temperature shot-noise power is given by

$$P = P_0\,\hat{\mathrm{T}}\mathrm{r}[\hat{t}\hat{t}^{\dagger}(\hat{1}-\hat{t}\hat{t}^{\dagger})], \tag{30}$$

where $P_0=2eVG_0$. Since the first term is proportional to the conductance, we just need to calculate the diagrams associated with the second moment $\hat{\mathrm{T}}\mathrm{r}[(\hat{t}\hat{t}^{\dagger})^2]$. A remarkable feature of the present stub model is the fact that we may import the diagrammatic structure of a similar calculation in the corresponding NNN system, obtained by substituting the ferromagnetic reservoirs by normal ones. These diagrams are available in Ref. 25. They are shown in Fig. 3 with the insertion of the spin degrees of freedom. All diagrams contain a central kernel attached to traces of the matrices $F^L_{\sigma_1\sigma_2}$ and $F^R_{\sigma_1\sigma_2}$, which are defined diagrammatically in Fig. 4. Except for the first diagram, all kernels are T cycles. Similarly to the conductance calculation, we represent these T cycles by matrices. So, we define the 16×16 matrix

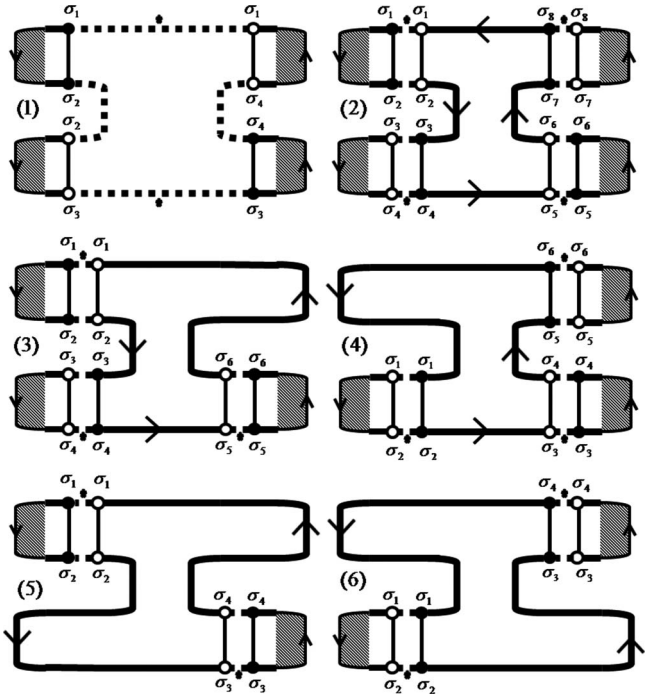

FIG. 3. Planar diagrams generated by averaging the term $\hat{\mathrm{T}}\mathrm{r}[(\hat{t}\hat{t}^{\dagger})^2]$.

$$\mathcal{T}^2_{s_1s_2} \equiv \mathrm{Tr}(R_{\sigma_1\sigma_2}R^{\dagger}_{\sigma_3\sigma_4}R_{\sigma_5\sigma_6}R^{\dagger}_{\sigma_7\sigma_8}), \tag{31}$$

the 16×4 matrices

$$\mathcal{T}^3_{s_1s_2} \equiv \mathrm{Tr}(B_{\sigma_1\sigma_2}R_{\sigma_3\sigma_4}R^{\dagger}_{\sigma_5\sigma_6}),$$

$$\mathcal{T}^4_{s_1s_2} \equiv \mathrm{Tr}(R^{\dagger}_{\sigma_1\sigma_2}R_{\sigma_3\sigma_4}A_{\sigma_5\sigma_6}), \tag{32}$$

and the 4×4 matrices

$$\mathcal{T}^5_{s_1s_2} \equiv \mathrm{Tr}(B_{\sigma_1\sigma_2}B_{\sigma_3\sigma_4}),$$

$$\mathcal{T}^6_{s_1s_2} \equiv \mathrm{Tr}(A_{\sigma_1\sigma_2}A_{\sigma_3\sigma_4}). \tag{33}$$

It is also convenient to define the vectors

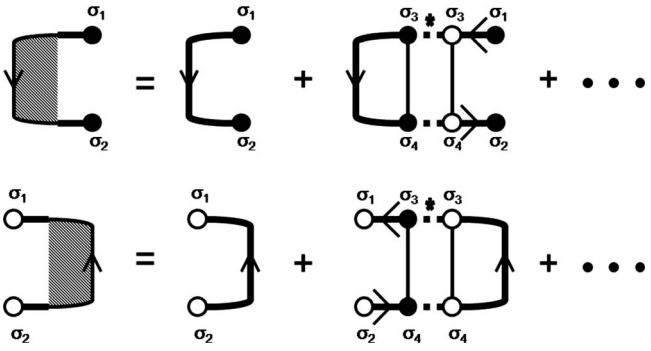

FIG. 4. Diagrammatic representation of $F^L_{\sigma_1\sigma_2}$ (top) and $F^R_{\sigma_1\sigma_2}$ (bottom).

TABLE I. Algebraic expressions for diagrams showed in Fig. 3 including its multiplicity.

1	$W_2\mathcal{F}^R\cdot\mathcal{T}^1\cdot(\mathcal{F}^R)^\top$
2	$W_1^4\mathcal{F}^{LR}\cdot\mathcal{T}^2\cdot(\mathcal{F}^{LR})^\top$
3	$2W_1^3\mathcal{F}^{LR}\cdot\mathcal{T}^3\cdot(\mathcal{F}^L)^\top$
4	$2W_1^3\mathcal{F}^{LR}\cdot\mathcal{T}^4\cdot(\mathcal{F}^R)^\top$
5	$W_1^2\mathcal{F}^L\cdot\mathcal{T}^5\cdot(\mathcal{F}^L)^\top$
6	$W_1^2\mathcal{F}^R\cdot\mathcal{T}^6\cdot(\mathcal{F}^R)^\top$

$$\mathcal{F}_s^L \equiv \mathrm{Tr}(F^L_{\sigma_1\sigma_2}),$$

$$\mathcal{F}_s^R \equiv \mathrm{Tr}(F^R_{\sigma_1\sigma_2}), \tag{34}$$

and

$$\mathcal{F}_s^{LR} \equiv \mathrm{Tr}(F^L_{\sigma_1\sigma_2})\mathrm{Tr}(F^R_{\sigma_3\sigma_4}). \tag{35}$$

For the first diagram, we define the 4×4 matrix

$$\mathcal{T}^1_{s_1s_2} \equiv \mathrm{Tr}(F^L_{\sigma_1\sigma_2}F^L_{\sigma_3\sigma_4}), \tag{36}$$

which does not represent a central kernel.

The matrix in Eq. (31), has rows and columns set by the indices $(\sigma_4,\sigma_5,\sigma_6,\sigma_7)$ and $(\sigma_1,\sigma_2,\sigma_7,\sigma_8)$, respectively. As for the matrix in Eq. (32), the rows are determined by $(\sigma_2\sigma_3\sigma_4\sigma_5)$ and the columns by $(\sigma_1\sigma_6)$. Although there is a great number of elements in the above defined matrices, just a few of them are independent. In particular, the matrix defined in Eq. (31) has just eleven independent elements. Note that we need second order γ parameters to calculate the matrices of Eqs. (31)–(33). The algebraic expressions corresponding to the diagrams in Fig. 3 are shown in Table I. The coefficients $W_1=1/N$ and $W_2=-1/N^3$ are used to account for the weight of each diagram. The multiplicity of each kind of diagram is also represented. For the sake of concreteness, let us analyze in more detail two particular, physically relevant cases. In both of them, we assume contacts with different polarizations.

1. Ideal ballistic contacts

Using the above diagrams the Fano factor, defined as the ratio $\langle P\rangle/2eV\langle G\rangle$, can be written as

$$F^{\mathrm{bal}}(\theta) = \frac{\sum_{n=0}^{8} E_n^{\mathrm{bal}} \sin^{2n}\left(\frac{\theta}{2}\right)}{\sum_{n=0}^{8} H_n^{\mathrm{bal}} \sin^{2n}\left(\frac{\theta}{2}\right)}, \tag{37}$$

where the coefficients E_n^{bal} and H_n^{bal} are polynomial functions of the polarization parameters p_a and p_b, which are shown in the Appendix. Note that the maximum value of $F^{\mathrm{bal}}(0)$ is 1/4, which corresponds to the Fano factor of a chaotic quantum dot coupled to two normal reservoirs. Note that for $\theta=0$, if we keep p_a fixed and vary p_b from p_a to 0 we observe that the Fano factor falls monotonically. On the other hand, if p_b is increased from p_a to 1, the Fano factor behaves nonmonotonically, passing through a minimum. These behaviors can be seen in Fig. 5. In the particular case of symmetric contacts, i.e., with the same number of open channels, Ref. 7 reported a critical value of the polarization, $p^c=1/3$, at which the monotonicity of the Fano factor with respect to $\cos\theta$ disappears. At this critical polarization a maximum in $F^{\mathrm{bal}}(\theta)$ appears at $\theta=0$, which moves toward $\theta=\pi$ as p varies from p^c to 1. This feature remains in the asymmetric case, as we show in Fig. 5 and in the diagram of Fig. 6. The solid line in this diagram separates the monotonic from the nonmono-

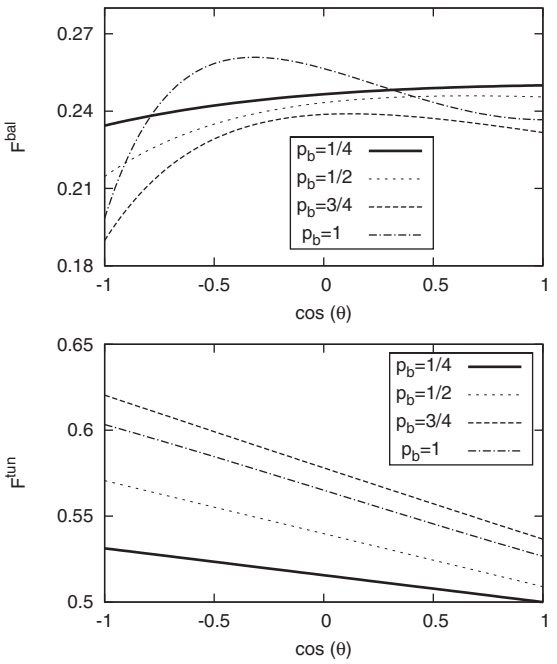

FIG. 5. Fano factor for ideal ballistic contacts (top) and tunnel junctions (bottom), in units of F_0. We fix $p_a=\frac{1}{4}$ and different values of p_b are considered in both cases.

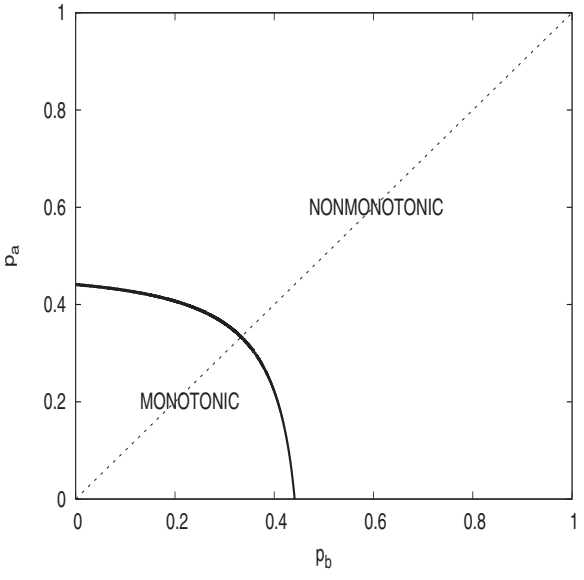

FIG. 6. Transition between monotonic and nonmonotonic behavior with respect to the angle between the magnetizations of the reservoirs. The dotted line represents the symmetric case.

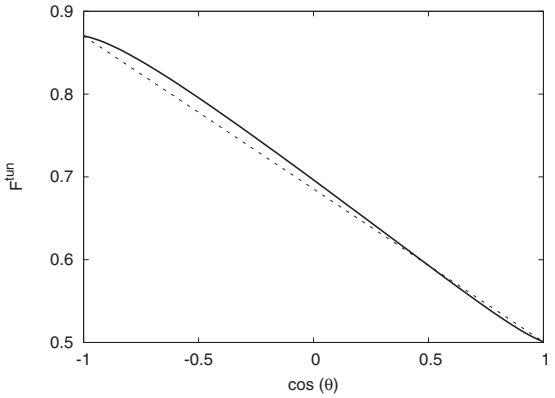

FIG. 7. Fano factor with tunnel junctions for $p_a=1$ and $p_b=17/20$ (solid line) and the interpolation between the values at collinear configurations (dotted lines).

tonic behavior. The dotted line represents the symmetric case.

2. Tunnel junctions

In this case the Fano factor is given by

$$F^{\mathrm{tun}}(\theta)=\frac{\sum_{n=0}^{5}E_n^{\mathrm{tun}}\sin^{2n}\left(\frac{\theta}{2}\right)}{\sum_{n=0}^{4}H_n^{\mathrm{tun}}\sin^{2n}\left(\frac{\theta}{2}\right)}, \tag{38}$$

where the coefficients E_n^{bal} and H_n^{bal} are shown in the Appendix. In the symmetric case Eq. (38) reduces to

$$F^{\mathrm{tun}}(\theta)=\frac{1}{2}\left(1+p^2\sin^2\frac{\theta}{2}\right), \tag{39}$$

in agreement with Ref. 7. Note that $F^{\mathrm{tun}}(0)$ reaches its minimum value of 1/2 when $p_a=p_b$, thus any difference between the polarizations tends to enhance the Fano factor. On the other hand, $F^{\mathrm{tun}}(\pi)$ can vary from a minimum value 1/2 to a maximum 1. Despite the complicated angular dependence of Eq. (38), the behavior of $F^{\mathrm{tun}}(\theta)$ as a function of cos θ for different polarizations is very similar to the above symmetric case, although the linear dependence is replaced by a weak nonlinear interpolation between the values at collinear configurations, as shown in the Fig. 7. We observed that the deviations from the linear interpolation is less than 3% (see Fig. 8). They are enhanced when one of the polarizations is close to 1. The relative deviation is defined by

$$D_R=\frac{|F^{\mathrm{tun}}(\theta)-Y(\theta)|}{Y(\theta)},$$

where $Y(\theta)$ is the linear interpolation function.

V. CONCLUSIONS

We introduced a stub model to describe a normal chaotic cavity connected to an arbitrary number of normal or noncollinear ferromagnetic reservoirs. For each contact a reduced set of parameters, sufficient to calculate any planar diagram, is defined and explicit expressions of this set are given for ideal ballistic contacts and tunnel junctions. The conductance and shot-noise power were explicitly calculated for a two terminal device with noncollinear ferromagnetic reservoirs. The general analytic expressions reproduce known results of the literature in the relevant limits. We analyzed in more detail the behavior of the shot-noise power in the case of contacts with different polarizations. We observed that the Fano factor exhibits a transition between monotonic and nonmonotonic behaviors as a function of the reservoir's relative magnetization angle. A diagram of this transition in the plane of the polarization parameters is shown.

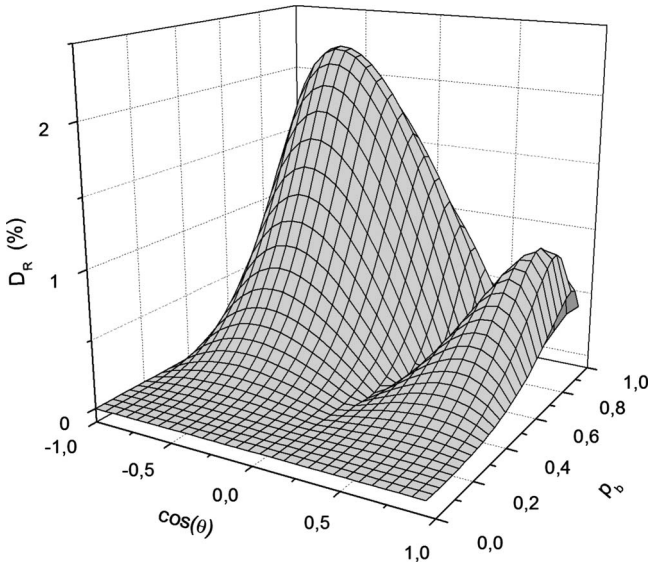

FIG. 8. Relative deviation of $F^{\mathrm{tun}}(\theta)$ with respect to a linear interpolation, fixing $p_a=1$.

There are a number of ways in which our approach can be extended. The central idea is to think of it as the most natural quantum-mechanical generalization of semiclassical circuit theory with probability amplitudes replacing probabilities in the concatenation rules and balance equations. An important point is that the effects of the spin-flip scattering (relevant in practical devices) and a magnetic field in the cavity could in principle be included without affecting the efficiency of the diagrammatic calculations through the introduction of an additional stub,[26] which can be manipulated in our formalism as an additional terminal. Other applications of our formalism include hybrid systems with superconductors, normal metals, and ferromagnetic reservoirs.

It is interesting to compare our approach with that of Ref. 13 since both address the problem of optimizing the random scattering matrix description to enhance its performance in comparison with quasiclassical techniques. While both approaches can calculate efficiently the conductance, the authors of Ref. 13 did not calculate the shot-noise power, which is the central result of our work and provides a crucial benchmark as far as calculational efficiency goes. On the other hand, the approach of Ref. 13 can deal very efficiently with spin-flip scattering and multilayer structures and we did not include these topics in our analysis. Finally, because of

its direct link with the diagrammatic technique our approach can also be used to calculate efficiently both weak-localization corrections and mesoscopic fluctuations, a problem which was not discussed in Ref. 13. In summary, we believe that these two random scattering matrix approaches complement each other nicely and both offer promising perspectives in the near future.

ACKNOWLEDGMENT

This work was partially supported by CNPq and FACEPE (Brazilian Agencies).

APPENDIX: MATRIX $\mathcal{L}$ AND TABLES OF COEFFICIENTS

The following symmetry requirements hold for the elements of the matrix $\mathcal{L}$:

$$\mathcal{L}_{12} = \mathcal{L}_{21} = \mathcal{L}_{13}^* = \mathcal{L}_{31}^*,$$

$$\mathcal{L}_{14} = \mathcal{L}_{41} = \mathcal{L}_{23} = \mathcal{L}_{32},$$

$$\mathcal{L}_{24} = \mathcal{L}_{42} = \mathcal{L}_{34}^* = \mathcal{L}_{43}^*,$$

TABLE II. Coefficients that contribute to $F^{\mathrm{bal}}(\theta)$.

$$E_0^{\mathrm{bal}}=2(p_a-2+p_b)(p_a^5p_b+p_a^4p_b^2-2p_a^4-2p_bp_a^3-4p_b^2p_a^2+p_a^2p_b^4+5p_a^2-2p_b^3p_a+p_b^5p_a+2p_bp_a-2p_b^4-4+5p_b^2)(p_a+p_b+2)^4$$

$$E_1^{\mathrm{bal}}=4p_bp_a(48+24p_a+24p_b-20p_a^5p_b-27p_a^4p_b^2+64p_bp_a^3+84p_b^2p_a^2-27p_a^2p_b^4+64p_b^3p_a-20p_b^5p_a-72p_bp_a+30p_a^4-68p_a^2+30p_b^4-68p_b^2+9p_b^4p_a-18p_a^3-18p_b^3-16p_a^3p_b^3-2p_b^2p_a^3-2p_b^3p_a^2+9p_a^4p_b-22p_b^2p_a-22p_bp_a^2+p_a^5+p_b^5-p_b^6-p_a^6+4p_a^4p_b^3+4p_b^4p_a^3+3p_a^5p_b^2+3p_a^2p_b^5+p_a^6p_b+p_b^6p_a)(p_a+p_b+2)^3$$

$$E_2^{\mathrm{bal}}=-4p_bp_a(64+80p_a+80p_b-102p_a^5p_b-193p_a^4p_b^2+372p_bp_a^3+372p_b^2p_a^2-193p_a^2p_b^4+372p_b^3p_a-102p_b^5p_a-416p_bp_a+42p_a^4-104p_a^2+42p_b^4-104p_b^2+294p_b^4p_a-92p_a^3-92p_b^3-196p_a^3p_b^3+396p_b^2p_a^3+396p_b^3p_a^2+294p_a^4p_b-388p_b^2p_a-388p_bp_a^2+30p_a^5+30p_b^5+p_b^6+p_a^6-104p_a^4p_b^3-104p_b^4p_a^3+28p_a^6p_b^2+35p_a^5p_b^3+28p_a^2p_b^6+p_a^7p_b-178p_a^5p_b^2-178p_a^2p_b^5+16p_a^4p_b^4+35p_a^3p_b^5-38p_a^6p_b-38p_b^6p_a+p_bp_a)(p_a+p_b+2)^2$$

$$E_3^{\mathrm{bal}}=16p_bp_a(p_a+p_b+2)(6p_a^5p_b-50p_a^4p_b^2+148p_bp_a^3+272p_b^2p_a^2-50p_a^2p_b^4+148p_b^3p_a+6p_b^5p_a-208p_bp_a+12p_a^4-16p_a^2+12p_b^4-16p_b^2+236p_b^4p_a-8p_a^3-8p_b^3+132p_a^3p_b^3+562p_b^2p_a^3+562p_b^3p_a^2+236p_a^4p_b-240p_b^2p_a-240p_bp_a^2+10p_a^5+10p_b^5+2p_b^6+2p_a^6-4p_a^5p_b^4-258p_a^4p_b^3-258p_a^3p_b^4-52p_a^6p_b^2+11p_b^7p_a^2+49p_a^3p_b^6-4p_a^4p_b^5-111p_a^5p_b^3+49p_a^6p_b^3-52p_a^2p_b^6-5p_a^7p_b-319p_a^5p_b^2-319p_a^2p_b^5+11p_a^7p_b^2-64p_a^4p_b^4-111p_a^3p_b^5-39p_a^6p_b-39p_b^6p_a-5p_b^7p_a)$$

$$E_4^{\mathrm{bal}}=-16p_bp_a(49p_a^5p_b+123p_a^4p_b^2+92p_bp_a^3+704p_b^2p_a^2+123p_a^2p_b^4+92p_b^3p_a+49p_b^5p_a-96p_bp_a+12p_a^4+12p_b^4+196p_b^4p_a+8p_a^3+8p_b^3+1014p_a^3p_b^3+1278p_b^2p_a^3+1278p_b^3p_a^2+196p_a^4p_b-128p_b^2p_a-128p_bp_a^2+6p_a^5+6p_b^5+p_b^6+p_a^6+5p_b^2p_a^8+47p_b^4p_a^6-418p_a^5p_b^4+81p_a^7p_b^3+81p_b^7p_a^3-624p_a^4p_b^3-624p_b^4p_a^3-372p_a^6p_b^2-18p_b^7p_a^2+5p_b^8p_a^2+12p_a^3p_b^6-186p_b^5p_a^5-418p_a^4p_b^5-833p_a^5p_b^3+12p_a^6p_b^3-372p_a^2p_b^6-11p_a^7p_b-794p_a^5p_b^2-794p_a^2p_b^5-18p_a^7p_b^2-848p_a^4p_b^4-833p_a^3p_b^5+47p_b^6p_a^4-30p_a^6p_b-30p_b^6p_a-11p_b^7p_a)$$

$$E_5^{\mathrm{bal}}=64p_a^3p_b^3(88+120p_a+120p_b+13p_a^5p_b+14p_a^4p_b^2-128p_bp_a^3-270p_b^2p_a^2+14p_a^2p_b^4-128p_b^3p_a+13p_b^5p_a+68p_bp_a-37p_a^4-14p_a^2-37p_b^4-14p_b^2+19p_b^4p_a-96p_a^3-96p_b^3-94p_a^3p_b^3-154p_b^2p_a^3-154p_b^3p_a^2+19p_a^4p_b-144p_b^2p_a-144p_bp_a^2-p_a^5-p_b^5)$$

$$E_6^{\mathrm{bal}}=-64p_a^3p_b^3(16-7p_b^4+24p_b+3p_a^5p_b+24p_a-18p_a^3-234p_b^2p_a^2+12p_a^4p_b^2-18p_b^3+3p_b^5p_a+12p_a^2p_b^4+14p_b^4p_a-20p_bp_a-56p_b^3p_a-82p_a^3p_b^3-126p_b^2p_a^3-7p_a^4-126p_b^3p_a^2+14p_a^4p_b-102p_b^2p_a-56p_bp_a^3-102p_bp_a^2)$$

$$E_7^{\mathrm{bal}}=258p_b^4p_a^4(p_a+1)(p_b+1)(p_b^2-8p_bp_a-6p_b+p_a^2-6-6p_a)$$

$$E_8^{\mathrm{bal}}=258p_a^4p_b^4(p_b+1)^2(p_a+1)^2$$

$$H_0^{\mathrm{bal}}=(p_a+p_b+2)^6(p_a^2+p_b^2-2)(p_a-2+p_b)^3$$

$$H_1^{\mathrm{bal}}=-4p_bp_a(7p_b^2-p_b-14+p_b^2p_a-p_a+p_bp_a^2+7p_a^2)(p_a-2+p_b)^2(p_a+p_b+2)^5$$

$$H_2^{\mathrm{bal}}=4p_bp_a(p_a-2+p_b)(p_a^4p_b+4p_a^4+27p_b^2p_a^3-p_a^3+80p_bp_a^3-31p_bp_a^2+8p_b^2p_a^2-24p_a^2+27p_b^3p_a^2+4p_a+80p_b^3p_a+p_b^4p_a-31p_b^2p_a-160p_bp_a-24p_b^2+4p_b^4+32-p_b^3+4p_b)(p_a+p_b+2)^4$$

$$H_3^{\mathrm{bal}}=-16p_b^2p_a^2(p_a+p_b+2)^3(21p_a^4+9p_a^4p_b+75p_b^2p_a^3-9p_a^3+122p_bp_a^3-111p_bp_a^2+42p_b^2p_a^2-126p_a^2+75p_b^3p_a^2+36p_a+122p_b^3p_a+9p_b^4p_a-111p_b^2p_a-244p_bp_a-126p_b^2+21p_b^4+168-9p_b^3+36p_b)$$

$$H_4^{\mathrm{bal}}=16p_b^2p_a^2(96+72p_a+72p_b+3p_a^5p_b+108p_a^4p_b^2+192p_bp_a^3-82p_b^2p_a^2+108p_a^2p_b^4+192p_b^3p_a+3p_b^5p_a-600p_bp_a+9p_a^4-60p_a^2+9p_b^4-60p_b^2+168p_b^4p_a-42p_a^3-42p_b^3+338p_a^3p_b^3+506p_b^2p_a^3+506p_b^3p_a^2+168p_a^4p_b-582p_b^2p_a-582p_bp_a^2+6p_a^5+6p_b^5)(p_a+p_b+2)^2$$

$$H_5^{\mathrm{bal}}=-64p_a^3p_b^3(-84-72p_a-72p_b+15p_bp_a^3+131p_bp_a^2+21p_b^3+110p_b^2p_a^2+131p_b^2p_a+27p_a^2+21p_a^3+50p_bp_a+27p_b^2+15p_b^3p_a)(p_a+p_b+2)^2$$

$$H_6^{\mathrm{bal}}=64p_a^3p_b^3(-16-14p_a-14p_b+3p_bp_a^3+82p_bp_a^2+4p_b^3+78p_b^2p_a^2+82p_b^2p_a+5p_a^2+4p_a^3+66p_bp_a+5p_b^2+3p_b^3p_a)(p_a+p_b+2)^2$$

$$H_7^{\mathrm{bal}}=-1792p_a^4p_b^4(p_b+1)(p_a+1)(p_a+p_b+2)^2$$

$$H_8^{\mathrm{bal}}=256p_a^4p_b^4(p_b+1)(p_a+1)(p_a+p_b+2)^2$$

TABLE III. Coefficients that contribute to $F^{\mathrm{tun}}(\theta)$.

$E_0^{\mathrm{tun}}=-16+p_b^6+3p_b^4p_a^2+3p_a^4p_b^2+8p_b^3p_a^3+24p_bp_a-16p_b^3p_a-16p_bp_a^3-12p_b^2p_a^2-2p_a^4+12p_a^2+12p_b^2-2p_b^4+p_a^6$
$E_1^{\mathrm{tun}}=-2p_bp_a(24-16p_b^2+12p_bp_a^3+12p_b^3p_a-16p_a^2-16p_bp_a-2p_b^3p_a^3+p_ap_b^5+p_bp_a^5)$
$E_2^{\mathrm{tun}}=-2p_b^2p_a^2(-12p_a^2-12p_b^2+4p_b^3p_a^3+2p_a^4p_b^2-22p_b^2p_a^2+24p_bp_a-p_a^4+16-p_b^4+2p_b^4p_a^2)$
$E_3^{\mathrm{tun}}=8p_b^3p_a^3(4+4p_b^2p_a^2+p_bp_a^3-12p_bp_a+p_b^3p_a)$
$E_4^{\mathrm{tun}}=-4p_b^4p_a^4(p_a^2+p_b^2+10p_bp_a-12)$
$E_5^{\mathrm{tun}}=16p_a^5p_b^5$
$H_0^{\mathrm{tun}}=(-2+p_a^2+p_b^2)(p_a+p_b+2)^2(p_a+p_b-2)^2$
$H_1^{\mathrm{tun}}=-2p_bp_a(p_a+p_b+2)(p_a+p_b-2)(p_bp_a^3+4p_a^2+2p_b^2p_a^2+p_b^3p_a-4p_bp_a-8+4p_b^2)$
$H_2^{\mathrm{tun}}=2p_b^2p_a^2(-48p_bp_a+12p_b^3p_a+22p_b^2p_a^2+12p_bp_a^3+p_b^4+p_a^4)$
$H_3^{\mathrm{tun}}=-16p_b^3p_a^3(4p_bp_a-4+p_b^2+p_a^2)$
$H_4^{\mathrm{tun}}=32p_b^4p_a^4$

$$\mathcal{L}_{22}=\mathcal{L}_{33}^{*}. \tag{A1}$$

There are just six free elements whose expressions are given below:

$$\mathcal{L}_{11}=N_a-G_a^{\uparrow\uparrow}+\cos^4\frac{\theta}{2}(N_b-G_b^{\uparrow\uparrow})+\sin^4\frac{\theta}{2}(N_b-G_b^{\downarrow\downarrow})+2\sin^2\frac{\theta}{2}\cos^2\frac{\theta}{2}[N_b-\mathrm{Re}(G_b^{\uparrow\downarrow})], \tag{A2}$$

$$\mathcal{L}_{22}=N_a-G_a^{\uparrow\downarrow}+\cos^4\frac{\theta}{2}(N_b-G_b^{\uparrow\downarrow})+\sin^4\frac{\theta}{2}[N_b-(G_b^{\uparrow\downarrow})^*]+\sin^2\frac{\theta}{2}\cos^2\frac{\theta}{2}(2N_b-G_b^{\uparrow\uparrow}-G_b^{\downarrow\downarrow}), \tag{A3}$$

$$\mathcal{L}_{44}=N_a-G_a^{\downarrow\downarrow}+\cos^4\frac{\theta}{2}(N_b-G_b^{\downarrow\downarrow})+\sin^4\frac{\theta}{2}(N_b-G_b^{\uparrow\uparrow})+2\sin^2\frac{\theta}{2}\cos^2\frac{\theta}{2}[N_b-\mathrm{Re}(G_b^{\uparrow\downarrow})], \tag{A4}$$

$$\mathcal{L}_{12}=\sin\frac{\theta}{2}\cos\frac{\theta}{2}\left\{\cos^2\frac{\theta}{2}(G_b^{\uparrow\downarrow}-G_b^{\uparrow\uparrow})-\sin^2\frac{\theta}{2}[(G_b^{\uparrow\downarrow})^*-G_b^{\downarrow\downarrow}]\right\}, \tag{A5}$$

$$\mathcal{L}_{24}=\sin\frac{\theta}{2}\cos\frac{\theta}{2}\left\{\cos^2\frac{\theta}{2}(G_b^{\downarrow\downarrow}-G_b^{\uparrow\downarrow})+\sin^2\frac{\theta}{2}[(G_b^{\uparrow\downarrow})^*-G_b^{\uparrow\uparrow}]\right\}, \tag{A6}$$

$$\mathcal{L}_{14}=\sin^2\frac{\theta}{2}\cos^2\frac{\theta}{2}[2\,\mathrm{Re}(G_b^{\uparrow\downarrow})-G_b^{\uparrow\uparrow}-G_b^{\downarrow\downarrow}]. \tag{A7}$$

The coefficients of Eq. (37) and (38) are shown in Tables II and III, respectively.

[1] G. A. Prinz, Science **282**, 1660 (1998).
[2] A. Brataas, G. E. W. Bauer, and P. J. Kelly, Phys. Rep. **427**, 157 (2006).
[3] J. C. Slonczewski, J. Magn. Magn. Mater. **159**, L1 (1996).
[4] G. E. W. Bauer, A. Brataas, Y. Tserkovnyak, and B. van Wees, Appl. Phys. Lett. **82**, 3928 (2003).
[5] Y. V. Nazarov, Superlattices Microstruct. **25**, 1221 (1999).
[6] A. Brataas, Y. V. Nazarov, and G. E. W. Bauer, Phys. Rev. Lett. **84**, 2481 (2000).
[7] Y. Tserkovnyak and A. Brataas, Phys. Rev. B **64**, 214402 (2001).
[8] B. Abdollahipour and M. Zareyan, Phys. Rev. B **73**, 214442 (2006).
[9] J. Fabian, A. Matos-Abiage, C. Ertler, P. Stano, and I. Zutic, Acta Phys. Slov. **57**, 565 (2007).
[10] D. Neumaier, K. Wagner, S. Geissler, U. Wurstbauer, J. Sadowski, W. Wegscheider, and D. Weiss, Phys. Rev. Lett. **99**, 116803 (2007); D. Neumaier, K. Wagner, U. Wurstbauer, M. Reinwald, W. Wegscheider, and D. Weiss, New J. Phys. **10**, 055016 (2008).
[11] L. P. Rokhinson, Y. Lyanda-Geller, Z. Ge, S. Shen, X. Liu, M. Dobrowolska, and J. K. Furdyna, Phys. Rev. B **76**, 161201(R) (2007).

[12] X. Waintal, E. B. Myers, P. W. Brouwer, and D. C. Ralph, Phys. Rev. B **62**, 12317 (2000).
[13] V. S. Rychkov, S. Borlenghi, H. Jaffres, A. Fert, and X. Waintal, Phys. Rev. Lett. **103**, 066602 (2009).
[14] A. L. R. Barbosa and A. M. S. Macêdo, Phys. Rev. B **71**, 235307 (2005).
[15] G. C. Duarte-Filho, A. F. Macedo-Junior, and A. M. S. Macêdo, Phys. Rev. B **76**, 075342 (2007).
[16] P. W. Brouwer and C. W. J. Beenaker, J. Math. Phys. **37**, 4904 (1996).
[17] P. W. Brouwer, J. N. H. J. Cremers, and B. I. Halperin, Phys. Rev. B **65**, 081302(R) (2002).
[18] M. L. Polianski and P. W. Brouwer, J. Phys. A **36**, 3215 (2003).
[19] M. L. Mehta, *Random Matrices* (Elsevier, Amsterdam, 2004).
[20] P. Forrester (unpublished).
[21] Y. V. Nazarov and Y. M. Blanter, *Quantum Transport: Introduction to Nanoscience* (Cambridge University Press, Cambridge, 2009).
[22] M. L. Mehta, *Matrix Theory* (Les Editions de Physique, Les Ulis Cedex, 1989).
[23] A. Brataas, Y. V. Nazarov, and G. E. W. Bauer, Eur. Phys. J. B **22**, 99 (2001).
[24] J. Manschot, A. Brataas, and G. E. W. Bauer, Phys. Rev. B **69**, 092407 (2004).
[25] J. G. G. S. Ramos, A. L. R. Barbosa, and A. M. S. Macêdo, Phys. Rev. B **78**, 235305 (2008).
[26] J. H. Cremers, P. W. Brouwer, and V. I. Fal'ko, Phys. Rev. B **68**, 125329 (2003).